Nuclear Science and Techniques (2026) 37:53
https://doi.org/10.1007/s41365-025-01879-x

Theory of laser-assisted nuclear fusion

Jin-Tao Qi[1] · Zhao-Yan Zhou[2] · Xu Wang[3,4]

Received: 24 April 2025 / Revised: 27 June 2025 / Accepted: 7 July 2025 / Published online: 20 January 2026

Abstract
The process of nuclear fusion in the presence of a laser field was theoretically analyzed. The analysis is applicable to most fusion reactions and different types of currently available intense lasers, from X-ray free-electron lasers to solid-state near-infrared lasers. Laser fields were shown to enhance the fusion yields, and the mechanism of this enhancement was explained. Low-frequency lasers are more efficient in enhancing fusion than high-frequency lasers. The calculation results show enhancements of fusion yields by orders of magnitude with currently available intense low-frequency laser fields. The temperature requirement for controlled nuclear fusion may be reduced with the aid of intense laser fields.

Keywords Nuclear fusion · Intense lasers · Enhancement of fusion

1 Introduction

Controlled nuclear fusion is an active research field with the ultimate goal of supplying sustainable and clean energy solutions to humans [1–5]. Yet, it is difficult to achieve the condition of self-sustained nuclear fusion (i.e., ignition) in laboratory environments, essentially due to the fact that nuclear fusion cross-sections are very small. To increase the cross-section, the nuclear fuel must be heated to very high temperatures, typically on the order of 10^7 K. Achieving and maintaining such high temperatures is challenging in practice. Therefore, it is sensible and meaningful to consider methods that may increase the fusion cross-section and reduce the temperature requirement.

The possibility of using advanced light sources to influence and enhance nuclear fusion yields has attracted attention recently [6–10]. These are interesting and timely attempts to observe rapid progress in light-source technologies, especially those with extremities in intensity or frequency (photon energy). Light sources with extreme intensities include the extreme light infrastructure (ELI) of Europe [11–13] and the superintense ultrafast laser facility (SULF) in Shanghai [14–16]. These lasers are expected to reach peak intensities on the order of 10^{23} W/cm^2 in the coming years. The frequency is in the near-infrared regime with very small single photon energies (approximately 1.5 eV). Light sources with extreme frequencies, notably synchrotron radiation and X-ray free-electron lasers [17, 18], are capable of generating light with photon energies of 1–10 keV. Recently, the feasibility of using these light sources to control nuclear processes has been explored, with investigations covering α decay [19–22], nuclear fission [23], and nuclear optical effects [24–30]. The scope of research also extends to particle generation (neutrons [31], protons [32], muons [33]), plasma-based cross-section measurements [34–36], isomeric excitation [37–41], and nuclear clock [42–44].

It is not unreasonable to expect that these light sources influence the nuclear fusion process. The relevant energy

This work was supported by the National Natural Science Foundation of China (Nos. 12405288, 12374241, 12474484, U2330401, and 12088101) and the Natural Science Foundation of Top Talent of SZTU (No. GDRC202526).

✉ Zhao-Yan Zhou
cnzhzhy@nudt.edu.cn

✉ Xu Wang
xwang@gscaep.ac.cn

[1] Shenzhen Key Laboratory of Ultraintense Laser and Advanced Material Technology, Center for Intense Laser Application Technology, and College of Engineering Physics, Shenzhen Technology University, Shenzhen 518118, China

[2] Department of Physics, National University of Defense Technology, Changsha 410073, China

[3] Graduate School, China Academy of Engineering Physics, Beijing 100193, China

[4] Southern Center for Nuclear-Science Theory, Institute of Modern Physics, Huizhou 516000, China

scale of controlled nuclear fusion is on the order of 1 keV ($= 1.16 \times 10^7$ K). For high-frequency light sources, the absorption of a single photon will increase the energy of the fusion system by an order of 1 keV. For low-frequency-high-intensity light sources, the simultaneous absorption of 1,000 photons will increase the energy of the fusion system by a similar amount, and it will be shown later that this is not difficult with intensities that are readily available nowadays.

Existing studies on this topic focus either on light sources with high frequencies [6, 7] or those with low frequencies [8, 9]. This is mainly due to the theoretical techniques used to address the problem. For example, Queisser et al. employ a Floquet scattering method [6], and Lv et al. adopt the Kramers-Henneberger approximation [7], both of which are feasible only for high frequencies. Several studies have comparatively discussed different approaches for laser-assisted nuclear fusion to a certain extent [45–49], with particular emphasis on laser frequencies in the X-ray regime. A comprehensive theoretical analysis applicable to both high and low laser frequencies is still lacking. Without an analysis that considers different laser frequencies on the same footing, conclusions cannot be drawn regarding the type of laser that would be most efficient in enhancing fusion. Is an X-ray free-electron laser more efficient in enhancing fusion than near-infrared lasers? One might think that the answer would be yes because the absorption of a single photon from an X-ray laser is equivalent to the absorption of 1,000 photons from a near-infrared laser. However, it will be shown that the answer is no.

Extending the theoretical foundations laid by previous studies on low-frequency laser fields [8], this study provides a unified theoretical framework that covers both high-frequency lasers, such as X-ray free-electron lasers, and low-frequency lasers, such as near-infrared solid-state lasers. Different lasers were treated on the same footing. Conclusions were drawn on the preferable laser parameters to enhance the fusion yields. The analysis is physically oriented with the aim of providing a physical understanding using the least possible numerical calculations. Fundamentally, the process of laser-assisted nuclear fusion is a complex many-body problem, and an *ab initio* calculation starting from quantum chromodynamics remains impossible. A feasible theoretical treatment inevitably involves approximations at different levels. A highly precise and numerically intense theoretical technique is not desirable at this stage.

The remainder of this paper is organized as follows: In Sect. 2, the effects of laser fields on each stage (region) of a nuclear fusion process are analyzed. The calculation results are presented in Sect. 3. Discussions on various aspects of our analyses are provided in Sect. 4. A summary and outlook are provided in Sect. 5 to conclude the article.

2 Analyses of the laser-assisted nuclear fusion process

2.1 Nuclear fusion without laser fields

We began with nuclear fusion in the absence of laser fields. The nuclear fusion process is usually divided into three regions according to the relative distance between the two nuclei, as illustrated in Fig. 1a. From the rest frame of one nucleus (noted nucleus 1 for convenience), the other nucleus (nucleus 2) is initially in region III with an asymptotic energy E, which is usually between 1 and 10 keV depending on the temperature of the fusion environment. As it approaches, nucleus 2 will reach a classical turning point, where the Coulomb repulsive energy between the two nuclei equals the energy E. Via the quantum tunneling effect, nucleus 2 enters and passes through region II with a small probability. In region I, the two nuclei are very close to each other, and fusion reactions occur. The spatial range of region I is on the order of 1 fm (10^{-15} m), and the spatial range of region II is on the order of 100 fm for the typical energies of controlled fusion research.

Indeed, a fusion cross-section is usually written in the following form corresponding to the three-region division [50]

$$\sigma(E) = S(E)\frac{1}{E}\exp\left(-\frac{B_{\mathrm{G}}}{\sqrt{E}}\right). \tag{1}$$

The first factor on the right hand side, $S(E)$, is the result of many-body nuclear physics in region I. The exponential factor is the result of the tunneling process occurring in region II [51]. The $1/E$ factor, called the geometrical factor, is related to region III. The constant B_{G} is known as the Gamow constant. For the deuteron-triton (DT) fusion reaction (D + T $\rightarrow$ ^{4}He + n + 17.6 MeV), $B_{\mathrm{G}} = 34.38\sqrt{\mathrm{keV}}$. An ab initio calculation of the function $S(E)$ is extremely demanding, if possible. For most purposes, including that of the current article, it suffices to adopt an empirical form [52]

$$S(E) = \frac{A_1 + E(A_2 + E(A_3 + EA_4))}{1 + E(B_1 + E(B_2 + E(B_3 + EB_4)))}, \tag{2}$$

where the parameters A_i and B_i are determined by fitting the experimental data. For DT fusion, the values of these parameters are given as follows [52]:

$$\begin{aligned} A_1 &= 6.927 \times 10^4, \quad A_2 = 7.454 \times 10^8, \\ A_3 &= 2.050 \times 10^6, \quad A_4 = 5.200 \times 10^4, \\ B_1 &= 6.380 \times 10^1, \quad B_2 = -9.95 \times 10^{-1}, \\ B_3 &= 6.981 \times 10^{-5}, \quad B_4 = 1.728 \times 10^{-4}. \end{aligned}$$

Note that these values are accompanied by the value of E in keV when Eq. (2) is employed. The DT fusion cross-section $\sigma(E)$ and the function $S(E)$ are shown in Fig. 1b and

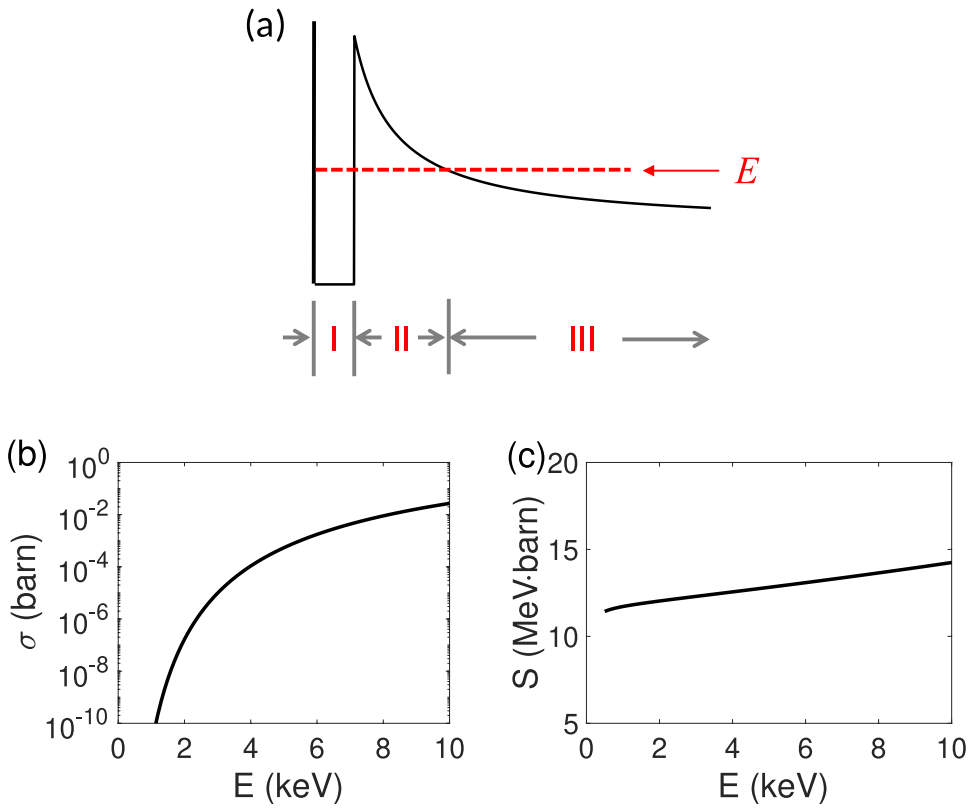

Fig. 1 **a** Schematic illustration of the three-region division of a nuclear fusion process. **b** The deuteron-triton fusion cross-section as a function of the relative collision energy E **c** The corresponding S function

c, respectively. $S(E)$ is a slow-varying function, whereas $\sigma(E)$ is an exponential function owing to the tunneling process. $\sigma(E)$ depends on E very sensitively, particularly for relatively low E values.

2.2 Two nuclei in a laser field, the center-of-mass reference frame

Now, let us consider the effects of an external laser field on the fusion process. Consider two nuclei with charge and mass $\{q_1, m_1\}$ and $\{q_2, m_2\}$ placed in a plane wave laser field. Two commonly used gauges are employed in light-matter interactions. One is the so-called velocity gauge, in which the laser field is characterized by a vector potential $\boldsymbol{A}(t)$. The total Hamiltonian is written as

$$H = \frac{1}{2m_1}\left[\boldsymbol{p}_1 - q_1\boldsymbol{A}(t)\right]^2 + \frac{1}{2m_2}\left[\boldsymbol{p}_2 - q_2\boldsymbol{A}(t)\right]^2 + \frac{q_1 q_2}{r}, \quad (3)$$

where $\boldsymbol{p}_1$ and $\boldsymbol{p}_2$ are the momenta of the two nuclei, and $r = |\boldsymbol{r}_1 - \boldsymbol{r}_2|$ is the distance between the two nuclei. Atomic units have been used, with $4\pi\epsilon_0 = 1$, hence the form of the Coulomb potential. We assumed the validity of the long-wavelength approximation by omitting the spatial dependency of the vector potential. This is justified by the fact that the spatial range relevant to nuclear fusion is much smaller than the wavelengths of the available intense lasers. Further discussion on this point is provided in Sect. 4.

For a fusion process, the relative motion between the two nuclei is the most relevant. Therefore, it is more convenient to work in the center-of-mass (CM) reference frame. Define

$$\boldsymbol{R} = \frac{m_1\boldsymbol{r}_1 + m_2\boldsymbol{r}_2}{m_1 + m_2}, \quad (4)$$

$$\boldsymbol{P} = \boldsymbol{p}_1 + \boldsymbol{p}_2, \quad (5)$$

$$\boldsymbol{r} = \boldsymbol{r}_1 - \boldsymbol{r}_2, \quad (6)$$

$$\boldsymbol{p} = \frac{m_2\boldsymbol{p}_1 - m_1\boldsymbol{p}_2}{m_1 + m_2}. \quad (7)$$

Then, after some straightforward algebra, the Hamiltonian in Eq. (3) can be rewritten as

$$H = \frac{1}{2M}[\boldsymbol{P} - Q\boldsymbol{A}(t)]^2 + \frac{1}{2\mu}\left[\boldsymbol{p} - q\boldsymbol{A}(t)\right]^2 + \frac{q_1 q_2}{r}, \quad (8)$$

where

$$M = m_1 + m_2, \quad (9)$$

$$\mu = \frac{m_1 m_2}{m_1 + m_2}, \tag{10}$$

$$Q = q_1 + q_2, \tag{11}$$

$$q = \frac{q_1 m_2 - q_2 m_1}{m_1 + m_2}. \tag{12}$$

One sees from Eq. (8), the Hamiltonian can be separated into the motion of the CM with charge and mass $\{Q, M\}$ and the motion of a virtual particle with charge and mass $\{q, \mu\}$. The mutual Coulomb potential is unaffected. The motion of the CM is not of concern here because it is not relevant to the fusion process.

Alternatively one may use the so-called length gauge and the Hamiltonian is given as

$$H = \frac{p_1^2}{2m_1} + \frac{p_2^2}{2m_2} + \frac{q_1 q_2}{r} - (q_1 \boldsymbol{r}_1 + q_2 \boldsymbol{r}_2) \cdot \boldsymbol{\mathcal{E}}(t), \tag{13}$$

where $\boldsymbol{\mathcal{E}}(t)$ denotes the laser electric field. Again, the long-wavelength approximation was assumed by neglecting the spatial dependency of the laser electric field. The above Hamiltonian can also be written in the CM reference frame as

$$H = \left[\frac{P^2}{2M} - Q\boldsymbol{R} \cdot \boldsymbol{\mathcal{E}}(t)\right] + \left[\frac{p^2}{2\mu} - q\boldsymbol{r} \cdot \boldsymbol{\mathcal{E}}(t)\right] + \frac{q_1 q_2}{r}. \tag{14}$$

The motion of the two nuclei is equivalent to the motion of the CM with $\{Q, M\}$ plus the motion of a virtual relative-motion particle with $\{q, \mu\}$.

2.3 Assumption on region I

The size of region I is on the order of 1 fm. In this region, the two nuclei fuse, and new particles are generated. For the DT fusion reaction, an α particle and a neutron are generated. This is a complex many-body nuclear process, and an *ab initio* treatment of this process is usually impossible. The addition of influences from an external laser field complicates the process.

However, it is reasonable to expect that the effect of the laser field in this region is negligibly. From the uncertainty principle, the spatial confinement of $\Delta x \sim 1$ fm $= 1.9 \times 10^{-5}$ a.u. indicates an uncertainty in momentum of $\Delta p \sim 5.3 \times 10^4$ a.u., or an uncertainty in energy of $(\Delta p)^2/2\mu \sim 6.4 \times 10^5$ a.u. ≈ 17 MeV. Here, $\mu = 2{,}204$ a.u. is the reduced mass of the deuteron and triton. In comparison, the effect of an intense laser field on the fusion process is on the order of 1 keV in energy, which is approximately four orders of magnitude smaller. It seems safe to neglect effects of external laser fields on the nuclear processes happening in region I. This is the basic assumption on which our analyses are based.

2.4 Effects of laser fields on region II

The size of region II is on the order of 100 fm. In this section, we show that an intense laser field has a finite but small effect on the tunneling process occurring in this region. The probability of tunneling, or the "penetrability", through a laser-modified Coulomb potential barrier can be calculated using the Wentzel-Kramers-Brillouin (WKB) method as

$$P(\theta, t) = \exp\left(-\frac{2}{\hbar}\int_{r_1}^{r_2} \sqrt{2\mu[V_{\mathrm{C}}(r) - E + V_{\mathrm{I}}(r, \theta, t)]}\,\mathrm{d}r\right), \tag{15}$$

where $V_{\mathrm{C}}(r) = q_1 q_2 / r$ is the Coulomb potential and $V_{\mathrm{I}}(r, \theta, t) = -q\boldsymbol{r} \cdot \boldsymbol{\mathcal{E}}(t) = -qr\mathcal{E}(t)\cos\theta$ is the laser-induced interaction potential from Eq. (14). Here, θ is the angle between the laser polarization direction and the DT collision (i.e., relative motion) direction. The integration is performed between two classical turning points, r_1 and r_2, which are also the two ends of region II.

What is implicit in writing Eq. (15) is a quasi-static approximation of the pressure. That is, the laser potential can be viewed as static at each time. This approximation is valid when the period of the laser field is much longer than the timescale of the tunneling process. More discussion on this point is provided in Sect. 4.

It can be estimated that the magnitude of V_{I} is much smaller than that of V_{C} or $V_0 \equiv V_{\mathrm{C}} - E$. The Coulomb potential V_{C} in region II can be estimated to be on the order of 100 keV, and the relative collision energy E is on the order of 1 keV in typical nuclear fusion experiments. With an intensity of 10^{20} W/cm^2, the magnitude of V_{I} can be estimated to be on the order of 10 eV. With an intensity of 10^{22} W/cm^2, the magnitude of V_{I} is approximately 100 eV. Therefore, we may expand Eq. (15) as

$$
\begin{aligned}
P(\theta,t) &= \exp\left(-\frac{2\sqrt{2\mu}}{\hbar}\int_{r_1}^{r_2}\sqrt{V_0}\sqrt{1+\frac{V_\mathrm{I}}{V_0}}\mathrm{d}r\right)\\
&\approx \exp\left(-\frac{2\sqrt{2\mu}}{\hbar}\int_{r_1}^{r_2}\sqrt{V_0}\left(1+\frac{V_\mathrm{I}}{2V_0}\right)\mathrm{d}r\right)\\
&= \exp\left(-\frac{2\sqrt{2\mu}}{\hbar}\int_{r_1}^{r_2}\sqrt{V_0}\mathrm{d}r\right)\\
&\quad\times\exp\left(-\frac{\sqrt{2\mu}}{\hbar}\int_{r_1}^{r_2}\frac{V_\mathrm{I}}{\sqrt{V_0}}\mathrm{d}r\right)\\
&\approx \exp\left(-\frac{2\sqrt{2\mu}}{\hbar}\int_{r_1}^{r_2}\sqrt{V_0}\mathrm{d}r\right)\\
&\quad\times\left(1-\frac{\sqrt{2\mu}}{\hbar}\int_{r_1}^{r_2}\frac{V_\mathrm{I}}{\sqrt{V_0}}\mathrm{d}r\right)\\
&= P(\mathcal{E}=0)\left(1+\gamma^{(1)}\right),
\end{aligned}
\tag{16}
$$

where $P(\mathcal{E}=0)$ is the penetrability without external laser fields, and $\gamma^{(1)}$ denotes the first-order correction induced by the laser field. Substituting the expression of V_I we get an explicit formula

$$
\gamma^{(1)}(\theta,t) = \frac{\sqrt{2\mu}}{\hbar}q\mathcal{E}(t)\cos\theta\int_{r_1}^{r_2}\frac{r}{\sqrt{V_0(r)}}\mathrm{d}r. \tag{17}
$$

The magnitude of $\gamma^{(1)}$ is maximum when $\mathcal{E}(t)$ reaches peaks and when $\cos\theta = 1$. The upper limit of integration r_2 is determined by equating the Coulomb potential $V_\mathrm{C}(r)$ to the collision energy E. For $E = 5$ keV, we get $r_2 = 288.3$ fm. The lower limit of integration r_1 is determined by a DT touching condition: $r_1 = r_\mathrm{D} + r_\mathrm{T} = 1.13(A_\mathrm{D}^{1/3} + A_\mathrm{T}^{1/3})$ fm $= 3.05$ fm. We find that for an intensity of 10^{20} W/cm^2, $\gamma^{(1)}$ takes a maximum value of 0.18%. For an intensity of 10^{22} W/cm^2, the maximum value was 1.8%. For $E = 10$ keV, $r_2 = 144.2$ fm. The corresponding maximum value of $\gamma^{(1)}$ is 0.03% for 10^{20} W/cm^2, and 0.3% for 10^{22} W/cm^2.

Therefore, one can see, for currently available state-of-the-art laser intensities, the effects of laser fields on region II are finite but small.

2.5 Effects of laser fields on region III

The major effects of a laser field on the fusion process originate from region III. The laser field can substantially influence the collision energy E.

Without external laser fields, the incoming relative-motion virtual particle is usually described asymptotically as a plane wave

$$
\psi(\boldsymbol{r},t) = \exp\left(i\boldsymbol{p}\cdot\boldsymbol{r} - iEt\right), \tag{18}
$$

where the momentum has a magnitude $p = \sqrt{2\mu E}$. This plane wave state has a well-defined energy E.

In the presence of a laser field, the asymptotic plane-wave state becomes a Volkov state [53]

$$
\psi_\mathrm{V}(\boldsymbol{r},t) = \exp\left[i\boldsymbol{p}\cdot\boldsymbol{r} - iEt - i\int_0^t H_\mathrm{I}(t')\mathrm{d}t'\right], \tag{19}
$$

where H_I is the interaction Hamiltonian with an external laser field. It is convenient to use the velocity gauge here, and from Eq. (8)

$$
H_\mathrm{I}(t) = -\frac{q}{\mu}\boldsymbol{p}\cdot\boldsymbol{A}(t) + \frac{q^2}{2\mu}A^2(t). \tag{20}
$$

Let us assume that the laser field is linearly polarized along the z axis, and the vector potential $\boldsymbol{A}(t) = \hat{z}A_0\sin\omega t$. The cases of elliptical or circular polarization are discussed in Sect. 4. Note that because the laser field can be very intense, the A^2 term cannot be simply ignored as in low-intensity cases.

The Volkov state can be expanded in terms of photon numbers

$$
\psi_\mathrm{V}(\boldsymbol{r},t) = \mathrm{e}^{i\boldsymbol{p}\cdot\boldsymbol{r}}\sum_{n=-\infty}^{\infty}\mathrm{e}^{iu}F_n(u,v)\mathrm{e}^{-i(E+U_\mathrm{p}+n\omega)t}, \tag{21}
$$

where the coefficient $F_n(u,v)$ is given by the following integral

$$
F_n(u,v) = \frac{1}{2\pi}\int_{-\pi}^{\pi}\mathrm{e}^{-iu\cos\xi+iv\sin 2\xi+in\xi}\mathrm{d}\xi. \tag{22}
$$

For convenience we have defined $U_\mathrm{p} = q^2A_0^2/4\mu$ (the ponderomotive energy), $u = u(\theta) = qpA_0\cos\theta/\mu\omega$, and $v = q^2A_0^2/8\mu\omega$. Here, θ is the angle between $\boldsymbol{p}$ and the $+z$ axis, and θ enters into the formalism through u. In a thermal environment, the direction between $\boldsymbol{p}$ and the laser polarization axis is random.

One sees from Eq. (21) that in the presence of a laser field, the collision energy is no longer a well-defined single value. Instead, the energy becomes a distribution, which is centered at $E + U_\mathrm{p}$ (ponderomotive shift) and separated by the photon energy. The energy of the particle can be higher or lower than $E + U_\mathrm{p}$, corresponding to the absorption or emission of photons. The probability of finding the system with energy $E_n = E + U_\mathrm{p} + n\omega$ is

$$
P_n(u,v) = \left|F_n(u,v)\right|^2. \tag{23}
$$

The total probability summing over the photon number n is equal to unity

$$\sum_{n=-\infty}^{\infty} P_n = 1. \tag{24}$$

3 Numerical results

3.1 Energy distribution with different laser parameters

The energy distribution P_n depends sensitively on the laser parameters, particularly the frequency (photon energy). At the same laser intensity, the energy distribution can vary significantly for lasers with different photon energies. This is illustrated in Fig. 2, which shows the energy distributions for six different photon energies under the same intensity. The bare collision energy without the laser fields was assumed to be 5 keV (corresponding to a temperature of 5.8×10^7 K).

One can see that for a high-frequency laser with a photon energy of 1 keV (1,000 eV), almost the entire population still has the original collision energy of 5 keV. The probability of absorbing (emitting) a photon and changing the energy to 6 keV (4 keV) is very small, with a value of 2.6×10^{-6}. This probability is not visually distinguishable on a linear scale, as shown in Fig. 2a. The probability of absorbing (emitting) two photons and changing the energy to 7 keV (3 keV) is on the order of 10^{-12}. It is very difficult to absorb (emit) energy from (to) a high-frequency laser field, even if the intensity is high. The probability of absorbing or emitting more photons exhibits a perturbative feature. That is, the probability decreases substantially as the number of photons increases.

As the photon energy decreases to 100 eV (Fig. 2b), the probability of absorbing (emitting) a photon increases to about 0.025. This indicates that 2.5% of the population has an energy of 5.1 keV, and another 2.5% has an energy of 4.9 keV. The probability of absorbing (emitting) two photons is on the order of 10^{-4}. As the photon energy decreased to 50 eV (Fig. 2c), the probability of absorbing (emitting) one photon is about 27%, and that of absorbing (emitting) two photons is about 3.3%. The probability of remaining with the original collision energy decreased to 39%.

As the photon energy decreased to 30 eV (Fig. 2d), the energy distribution shows clear nonperturbative features. For example, the probability of absorbing (emitting) two photons is higher than that of absorbing (emitting) a single photon. The number of photons absorbed or emitted was approximately 5, and the energy range populated was approximately 4.85−5.15 keV.

As the photon energy decreases to 10 eV (Fig. 2e), the number of photons absorbed or emitted is about 40. The populated energy range was between 4.6 and 5.4 keV. In addition, the distribution shows an overall structure with peaks near the two ends and a valley in the middle. This indicates that the collision has substantial probabilities with energies away from the original bare energy. As the photon

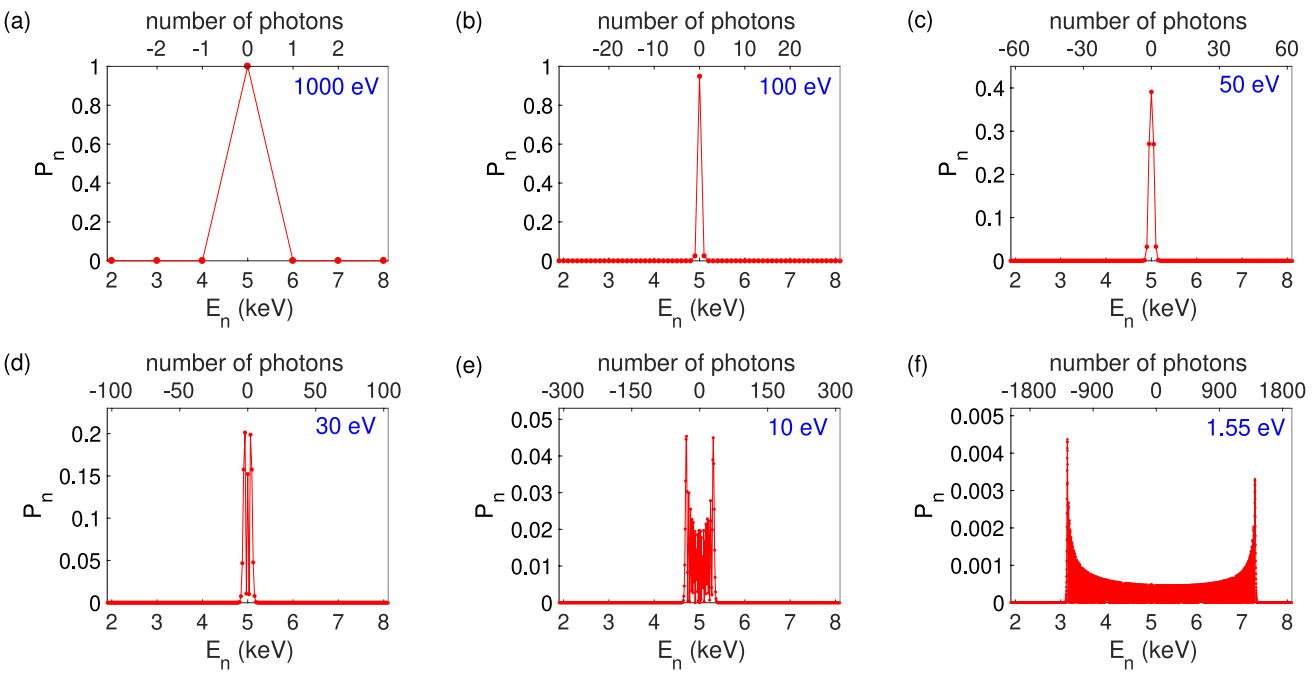

Fig. 2 Energy distributions of the Volkov state with different laser photon energies (frequencies) as labeled on the upper-right corner of each figure. The lasers were assumed to have the same intensity of 10^{20} W/cm^2. The bare collision energy E without the laser field is set to be 5 keV for all the cases

energy decreased to 1.55 eV (Fig. 2f), which corresponds to a wavelength of 800 nm from Ti:sapphire intense lasers, the number of photons absorbed or emitted is over 1,300, and energy range between 3.1 and 7.3 keV is substantially populated. In this case, the ponderomotive shift $U_p = 109$ eV and the distribution is not exactly symmetric.

The main message from the above results is that it is easier for low-frequency lasers to deliver energy to a fusion system. Although the energy of a single photon is small, the number of participating photons can be very large, so the populated energy range is wide.

Note that the energy distribution P_n depends on the parameter u, which depends on the angle θ between the laser polarization direction and collision (relative motion) direction. We set $\theta = 0°$ for all cases shown in Fig. 2. As θ increases from 0° to 90°, the energy distribution becomes narrower, as shown in Fig. 3 for the case of 1.55 eV (800 nm). P_n for $\theta > 90°$ is the same as that for $(180° - \theta)$. It is easier for the laser to deliver energy to the fusion system if the axis of collision and the axis of laser polarization are aligned.

3.2 Enhancement of fusion

In the presence of a laser field, the collision energy E changes from a single value to a distribution, the character of which depends on the laser parameters. The fusion system can either absorb energy from the laser field, leading to collision energies higher than E, or lose energy to the laser field, leading to energies lower than E (the center of the energy distribution is shifted to $E + U_p$). Energies higher than E lead to higher fusion yields, and energies lower than E lead to lower fusion yields.

However, the net effect is an enhancement of the fusion yield. This is because the cross-section function in Eq. (1) depends exponentially on the collision energy (concave upward), as shown in Fig. 4 in linear scale. The fusion yields gained at higher energies are greater than those lost at lower energies. This is the mechanism of fusion-yield enhancement in the presence of laser fields.

3.3 Effective fusion cross-section

It is sensible to define an effective fusion cross-section in the presence of a laser field. We denote this laser-assisted cross-section as $\sigma_L(E)$, which can be calculated by averaging over all θ angles between the collision direction and the laser polarization direction

$$\sigma_L(E) = \frac{1}{2}\int_0^\pi \sigma_L(E,\theta)\sin\theta \mathrm{d}\theta, \tag{25}$$

where $\sigma_L(E,\theta)$ is defined as

$$\sigma_L(E,\theta) = \sum_{n=-\infty}^{\infty} P_n[u(\theta), v]\sigma(E + U_p + n\omega). \tag{26}$$

The effective cross-section $\sigma_L(E)$, in comparison with the laser-free cross-section $\sigma(E)$, provides a quantitative

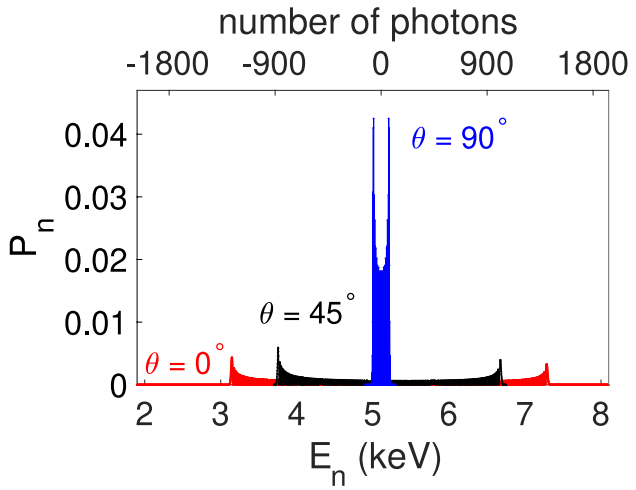

Fig. 3 (Color online) Energy distributions for three different θ angles, as labeled on figure, between the laser polarization direction and the DT collision direction. The laser has a photon energy of 1.55 eV (wavelength of 800 nm) and an intensity of 10^{20} W/cm^2. The 0° case is the same as Fig. 2f

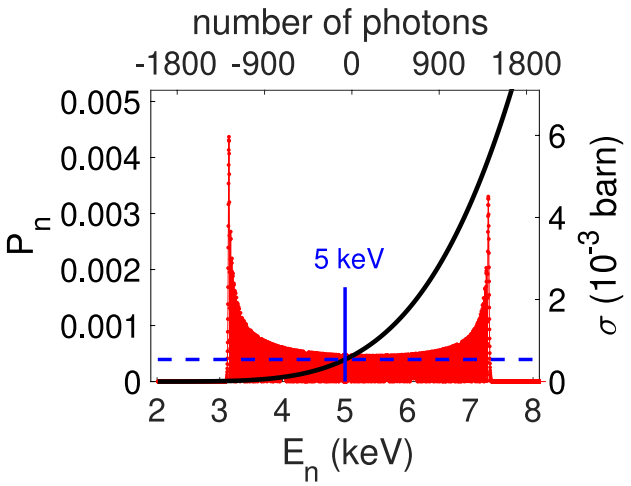

Fig. 4 (Color online) Illustration of fusion enhancement in a laser field. Without laser fields, the bare collision energy is assumed to be 5 keV, corresponding to a fusion cross-section of 0.538×10^{-3} barn (dashed horizontal line). In the presence of a laser field, the collision energy becomes a distribution (an example is shown as the red curve on the left axis), with energies higher and lower than 5 keV. Higher energies lead to higher fusion yields, whereas lower energies lead to lower fusion yields. However, the fusion yields gained with higher energies are greater than the fusion yields lost with lower energies because the cross-section function is an exponential function, concaving upward (black solid curve, right axis)

measure of the effect of a laser field on the nuclear fusion process. It should be emphasized that the laser field mainly affects the fusion process by modifying the collision energy in region III before the tunneling process. It has very small effects on the processes occurring in regions I and II, as explained above.

Figure 5 shows the laser-assisted effective DT fusion cross-section for three bare energies ($E = 1$, 5, and 10 keV) and different laser intensities and photon energies. These three energies represent the typical temperatures in thermonuclear fusion experiments. One sees from Fig. 5 that to have noticeable effects on nuclear fusion, the laser intensity needs to be higher than 10^{18} or 10^{19} W/cm^2.

One can also see that σ_L is larger for lower laser frequencies at the same intensity. For all three cases and with the intensity range shown, the fusion enhancement for the higher frequency cases (100 eV and 1,000 eV) is very small. This is the direct consequence of the point explained above, that low-frequency lasers are more efficient in delivering energy to the fusion system. It is difficult to absorb energy from high-frequency laser fields.

Substantial enhancements can be observed with low-frequency 1.55 eV lasers. For $E = 1$ keV, the enhancement is three orders of magnitude at an intensity of 10^{20} W/cm^2 and nine orders of magnitude at an intensity 5×10^{21} W/cm^2. The enhancement ratio decreases as E increases. This is because the cross-section function $\sigma(E)$ in Eq. (1) is more sensitive to E for smaller E values. The effect of the laser field was more pronounced for smaller E values.

The possibility of using lasers to reduce the temperature requirements of fusion reactions is evident. For example, without laser fields, the DT fusion cross-section at $E = 1$ keV is 1.37×10^{-11} barn. With an 800-nm (1.55-eV) laser field of intensity 10^{20} W/cm^2, the effective fusion cross-section becomes 1.02×10^{-8} barn, which is equal to the cross-section value at $E = 1.6$ keV without laser fields. If the laser intensity is 5×10^{21} W/cm^2, the effective cross-section becomes 0.027 barn, which is equal to the cross-section value at $E = 10$ keV without laser fields. In other words, the enormous gap in the DT fusion cross-section between 1 keV (1.16×10^7 K) and 10 keV (1.16×10^8 K) is filled or compensated completely by the intense laser field.

4 Discussions

4.1 Applicability to other fusion reactions

Although the results presented above are for the DT fusion reaction, our analyses also apply to other fusion reactions, such as the neutronless proton-boron (p-^{11}B) fusion reaction [54–58], which is limited in its practical application because of its significantly lower fusion cross-section compared to that of DT fusion under low bare energy conditions.

The p-^{11}B interaction exhibits a larger effective charge, $q = 0.5$, in contrast to the value of $q = 0.2$ for the deuteron-triton (DT) system. Furthermore, the reduced mass for the p-^{11}B pair is notably smaller, with $\mu \approx 1683.2$ a.u., compared to $\mu \approx 2203.4$ a.u. for the DT pair. Consequently, under identical laser parameters, the ponderomotive energy, given by $U_p = q^2 A_0^2/4\mu$, was higher for the p-^{11}B system than for the DT system. The parameters $u = qpA_0 \cos\theta/\mu\omega$ and $v = q^2 A_0^2/8\mu\omega$ indicate that a greater number of photons are absorbed or emitted by the p-^{11}B pair compared to the DT pair in laser fields.

Figure 6a illustrates that the energy distribution of the Volkov state for the p-^{11}B system is broader than that of the DT system, as depicted in Fig. 3. The laser was characterized by a photon energy of 1.55 eV and a peak intensity of 10^{20} W/cm^2. Figure 6b presents the laser-assisted effective cross-section for p-^{11}B fusion as a function of bare collision energy, assuming a laser photon energy of 1.55 eV. Various laser intensities were considered, as indicated in the figure. The cross-section in the absence of laser fields is given in Ref. [59], is indicated by the black dashed line. Notably,

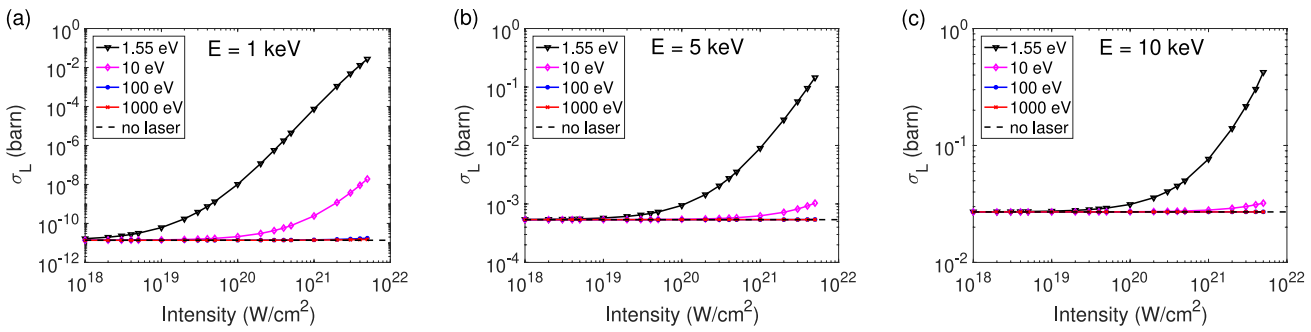

Fig. 5 (Color online) Laser-assisted effective DT fusion cross-sections for bare energies **a** 1, **b** 5, and **c** 10 keV. For each case, different laser intensities and photon energies were used, as labeled in the figure. The cross-section values without laser fields are marked in each figure as a horizontal-dashed line

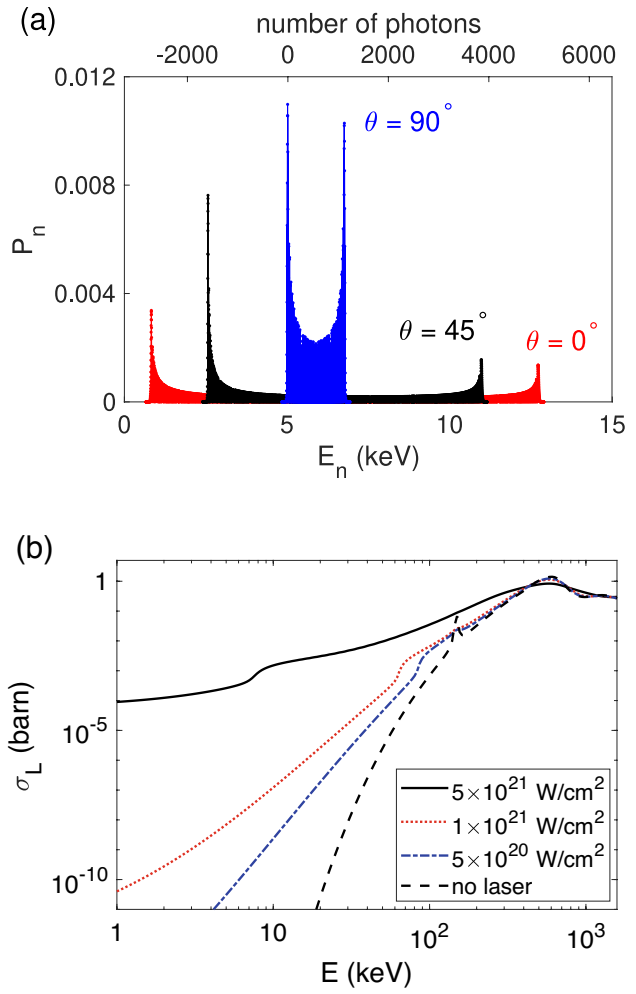

Fig. 6 (Color online) **a** Energy distribution of the Volkov state for p-^{11}B fusion reaction. θ denotes the angle between the laser polarization direction and the p-^{11}B collision direction. The laser had a photon energy of 1.55 eV and a peak intensity of 10^{20} W/cm^2. **b** Laser-assisted effective p-^{11}B fusion cross-sections as a function of bare collision energy, assuming a laser frequency of 1.55 eV. The results for different laser intensities are shown. The black-dashed line denotes the cross-section in the absence of the laser field

under the influence of a strong laser field with an intensity of 5×10^{21} W/cm^2, the effective cross-section of p-^{11}B fusion can reach the order of 10^{-4} barn in the bare energy range of 1–10 keV, representing a significant enhancement in fusion reactivity. The resonant peak of the p-^{11}B fusion cross-section, originally located at approximately 150 keV, shifts toward a lower and broader bare energy range under the influence of the laser field. This further indicates an effective enhancement of the fusion reactivity. These results highlight the potential of laser-assisted p-^{11}B fusion as a promising pathway for future research and development in clean, radiation-free energy generation.

However, laser fields have no effect, at least within the approximations adopted in this study, on fusion reactions with two nuclei having the same charge-to-mass ratio. An example of this type is the deuteron-deuteron fusion reaction. If so, one can find from Eq. (12) that the charge of the relative-motion virtual particle is zero and the laser ceases to have an effect on the relative-motion degree of freedom. This is easily understood because the motion of a charged particle in a laser field is determined by its charge-to-mass ratio. If two nuclei have the same charge-to-mass ratio, then their motion in the laser field will be the same, and the laser field has no tendency to separate them apart or press them closer, that is, the laser field has no effect on the relative motion between the two nuclei.

4.2 The long-wavelength approximation

We assumed the validity of the long-wavelength approximation by neglecting the spatial dependency of the laser vector potential or the electric field. This is justified if the spatial range relevant to fusion is significantly smaller than the laser wavelength. The former range can be estimated by the quiver motion amplitude $z_0 = qA_0/\mu\omega$, which is the amplitude of spatial oscillations of a free charged particle in a laser field. The required validity condition of the long-wavelength approximation is

$$\frac{qA_0}{\mu\omega} \ll \lambda = \frac{2\pi c}{\omega}, \quad \text{or} \quad A_0 \ll \frac{2\pi c\mu}{q}. \tag{27}$$

Putting in the values of μ and q for the DT fusion we get $A_0 \ll 9.5 \times 10^6$ a.u., or the amplitude of the laser electric field $E_0 = A_0\omega \ll 9.5 \times 10^6\omega$ in a.u.. We provide two examples. For photon energy 1,000 eV, $\omega = 36.8$ a.u., so $E_0 \ll 3.5 \times 10^8$ a.u. or equivalently the intensity $I \ll 4.3 \times 10^{33}$ W/cm^2. For photon energy 1.55 eV, $\omega = 0.0569$ a.u., so $E_0 \ll 5.4 \times 10^5$ a.u. or equivalently the intensity $I \ll 1.0 \times 10^{28}$ W/cm^2. The validity of the long-wavelength approximation can be guaranteed for both the examples.

4.3 The quasi-static approximation

As mentioned in Sect. 2.4, when writing Eq. (15), we have implicitly used the quasi-static approximation. This approximation is valid when the laser period is much longer than the time scale of the tunneling process, which can be estimated using a classical model. For example, for $E = 5$ keV, the velocity of relative motion is $v = \sqrt{2E/\mu} = 0.41$ a.u. The tunneling length (from the tunneling entrance point to the tunneling exit point) is 5.38×10^{-3} a.u. (285 fm), and the estimated time for the tunneling process is 0.013 a.u. or 0.32 as (1 as $= 10^{-18}$ s). The quasi-static approximation is valid as long as the laser period is much longer than 0.32 as or the photon energy is much lower than 13 keV.

We note that the quasi-static approximation is also an important concept in strong-field atomic ionization [60, 61]. The ratio between the classically estimated electron tunneling time and the laser period is called the Keldysh parameter [60]. The quasi-static approximation is valid when the Keldysh parameter $\gamma \ll 1$, that is, the tunneling time scale is much shorter than the laser period.

4.4 The Coulomb Volkov state

For simplicity, we used the (plane-wave) Volkov state to describe the relative motion of the virtual particle. The Volkov state is the solution to the time-dependent Schrödinger equation for a free charged particle in the presence of a laser field. The Coulomb potential between the two nuclei was neglected.

The quantum state of the full Coulomb-plus-laser system does not have a general analytical solution. An approximate solution is the Coulomb-Volkov state [62, 63], which has the same form as the plane-wave Volkov state, except that replace the $e^{i\boldsymbol{p}\cdot\boldsymbol{r}}$ in Eqs. (19) or (21) with a Coulomb wave function $\phi_{\boldsymbol{p}}(\boldsymbol{r})$. The temporal part, and hence the energy distribution, remained the same. Therefore, the results and discussions presented above are not affected if Coulomb Volkov states are used.

4.5 Elliptical or circular polarization

The extension of the above formalism to elliptically or circularly polarized laser fields is straightforward; therefore, we only outline a few steps here. Assuming that the vector potential is in the z-y plane: $\boldsymbol{A}(t) = \hat{z}A_\varepsilon \sin\omega t + \hat{y}\varepsilon A_\varepsilon \cos\omega t$, with ellipticity ε and amplitude $A_\varepsilon = A_0/\sqrt{1+\varepsilon^2}$. The Volkov wavefunction can then be written in the same form as Eq. (21), except that $F_n = F_n(u, w, v)$ has an additional argument w owing to the additional polarization direction. Here $u = u(\theta) = qpA_\varepsilon \cos\theta/\mu\omega$, $w = w(\theta, \phi) = qp\varepsilon A_\varepsilon \sin\theta \sin\phi/\mu\omega$, and $v = q^2A_\varepsilon^2(1-\varepsilon^2)/8\mu\omega$. (θ, ϕ) are the direction angles of momentum $\boldsymbol{p}$. The coefficient F_n is obtained via the integral

$$F_n(u, w, v) = \frac{1}{2\pi}\int_{-\pi}^{\pi} e^{-iu\cos\xi + iw\sin\xi + iv\sin 2\xi + in\xi} d\xi. \quad (28)$$

Because elliptical polarization breaks the cylindrical symmetry of linear polarization, the effective fusion cross-section σ_L must be averaged over both θ and ϕ. Figure 7 shows how the angle-averaged σ_L changes with ε for intensity 1×10^{20} W/cm^2. Elliptical or circular polarization did not lead to further enhancements in the fusion yield. The efficiency is (slightly) lower than that of linear polarization, mainly because of the reduction in the field amplitude from A_0 to A_ε.

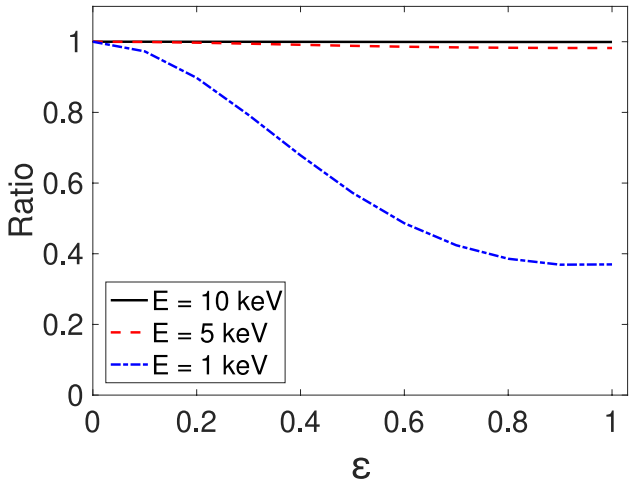

Fig. 7 (Color online) Dependency of angle-averaged effective fusion cross-section σ_L on laser ellipticity ε, for three bare energies 1, 5, and 10 keV under intensity 1×10^{20} W/cm^2. For each case, σ_L has been normalized to the corresponding value of linear polarization

4.6 Effects of plasma screening

In laser-induced plasmas, the range of charge screening effects can be characterized by a Debye sphere, with a radius given by the Debye length $\lambda_D \approx 740\sqrt{T_e/n_e}$, where λ_D is in cm, T_e is in eV, and n_e is in units of cm^{-3}. Plasma screening becomes significant when the internuclear separation exceeds the Debye length, because the Coulomb interaction is substantially shielded by the surrounding plasma electrons. Conversely, when the internuclear distance is shorter than the Debye length, the screening effect is relatively weak, and the bare nuclear interaction dominates.

Assuming a plasma electron temperature of 2 keV and electron density of 10^{17} cm^{-3}, the corresponding Debye length is approximately 1 μm. This characteristic length scale is significantly larger than the amplitude of the quiver motion between two nuclei in a laser field with an intensity of 5×10^{21} W/cm^2 and a photon energy of 1.55 eV, which is approximately 0.56 nm. Consequently, the internuclear separation remains well below the Debye length, and the influence of plasma screening is negligible. Therefore, the two-nuclei interaction model employed in this study is well justified in disregarding the effects of the plasma screening.

The plasma environment may also involve additional effects, such as collisional interactions and radiation processes, which can be further investigated through advanced laser-plasma simulations in future studies.

5 Summary and outlook

In summary, we considered the nuclear fusion process in the presence of a laser field. In the absence of laser fields, a nuclear fusion process is typically treated as a three-region process, and we analyzed the effects of laser fields on each of the three regions. Our analysis is physically oriented, aiming to provide a clear physical understanding of the laser-assisted nuclear fusion process. We show that the major effects of the laser field on the nuclear fusion process originate from influencing the collision energy before tunneling. We explain why this influence of the collision energy leads to enhanced fusion yields. By treating lasers with different frequencies on the same footing, we can draw conclusions regarding the optimal laser parameters to enhance fusion. We show that intense low-frequency lasers are the most efficient in delivering energy to the fusion system and enhancing the fusion yield.

The possibility is pointed out that lasers may be used to reduce the temperature requirement of controlled fusion research. The vast difference between the fusion cross-sections at different temperatures decreases in the presence of laser fields. Controlled fusion experiments can be performed at lower temperatures with the aid of intense laser fields.

In this study, we only consider the (pure) system of two nuclei plus a laser field. We did not consider a more complicated plasma environment with nuclei, electrons, laser-plasma interactions, etc. These complications are important but are outside the scope of the current study. As the first step, we need to understand the laser-assisted nuclear fusion process, which is the goal of the current study. The next step is to add the above-mentioned complications and evaluate the effect of laser fields.

Author Contributions All authors contributed to the study conception and design. Material preparation, data collection, and analysis were performed by Jin-Tao Qi, Zhao-Yan Zhou, and Xu Wang. The first draft of the manuscript was written by Jin-Tao Qi and all authors commented on previous versions of the manuscript. All authors read and approved the final manuscript.

Data Availability The data that support the findings of this study are openly available in Science Data Bank at https://cstr.cn/31253.11.sciencedb.j00186.00845 and https://www.doi.org/10.57760/sciencedb.j00186.00845.

Declarations

Conflict of interest The authors declare that they have no conflict of interest.

References

1. F.L. Hinton, R.D. Hazeltine, Theory of plasma transport in toroidal confinement systems. Rev. Mod. Phys. **48**, 239 (1976). https://doi.org/10.1103/RevModPhys.48.239
2. J. Sheffield, The physics of magnetic fusion reactors. Rev. Mod. Phys. **66**, 1015 (1994). https://doi.org/10.1103/RevModPhys.66.1015
3. J.D. Lindl, P. Amendt, R.L. Berger et al., The physics basis for ignition using indirect-drive targets on the National Ignition Facility. Phys. Plasmas **11**, 339 (2004). https://doi.org/10.1063/1.1578638
4. O.A. Hurricane, D.A. Callahan, D.T. Casey et al., Fuel gain exceeding unity in an inertially confined fusion implosion. Nature **506**, 343 (2014). https://doi.org/10.1038/nature13008
5. R. Betti, O.A. Hurricane, Inertial-confinement fusion with lasers. Nat. Phys. **12**, 435 (2016). https://doi.org/10.1038/nphys3736
6. F. Queisser, R. Schützhold, Dynamically assisted nuclear fusion. Phys. Rev. C **100**, 041601(R) (2019). https://doi.org/10.1103/PhysRevC.100.041601
7. W. Lv, H. Duan, J. Liu, Enhanced deuterium-tritium fusion cross sections in the presence of strong electromagnetic fields. Phys. Rev. C **100**, 064610 (2019). https://doi.org/10.1103/PhysRevC.100.064610
8. X. Wang, Substantially enhanced deuteron-triton fusion probabilities in intense low-frequency laser fields. Phys. Rev. C **102**, 011601(R) (2020). https://doi.org/10.1103/PhysRevC.102.011601
9. B. Wu, Z. Fan, D. Ye et al., Multiphoton fusion of light nuclei in intense laser fields. Phys. Rev. C **109**, 064615 (2024). https://doi.org/10.1103/PhysRevC.109.064615
10. S. Liu, H. Duan, J. Liu, Deuterium-tritium fusion process in strong laser fields: Semiclassical simulation. Phys. Rev. C **104**, 044614 (2021). https://doi.org/10.1103/PhysRevC.104.044614
11. C.A. Ur, D. Balabanski, G. Cata-Danil et al., The ELI–NP facility for nuclear physics. Nucl. Instrum. Methods Phys. Res. B **355**, 198 (2015). https://doi.org/10.1016/j.nimb.2015.04.033
12. D.L. Balabanski, R. Popescu, D. Stutman et al., New light in nuclear physics: the extreme light infrastructure. Europhys. Lett. **117**, 28001 (2017). https://doi.org/10.1209/0295-5075/117/28001
13. D.L. Balabanski, P. Constantin, A. Rotaru et al., Status of ELI-NP and opportunities for hyperfine research. Hyperfine Interact. **240**, 49 (2019). https://doi.org/10.1007/s10751-019-1594-7
14. W. Li, Z. Gan, L. Yu et al., 339 J high-energy Ti: sapphire chirped-pulse amplifier for 10 PW laser facility. Opt. Lett. **43**, 5681 (2018). https://doi.org/10.1364/ol.43.005681
15. L. Yu, Y. Xu, Y. Liu et al., High-contrast front end based on cascaded XPWG and femtosecond OPA for 10-PW-level Ti:sapphire laser. Opt. Express **26**, 2625 (2018). https://doi.org/10.1364/oe.26.002625
16. Z. Zhang, F. Wu, J. Hu et al., The laser beamline in SULF facility. High Power Laser Sci. Eng. **8**, E4 (2020). https://doi.org/10.1017/hpl.2020.3
17. B.W.J. McNeil, N.R. Thompson, X-ray free-electron lasers. Nat. Photon. **4**, 814 (2010). https://doi.org/10.1038/nphoton.2010.239
18. P. Bucksbaum, N. Berrah, Brighter and faster: the promise and challenge of the X-ray free-electron laser. Phys. Today **68**(7), 26 (2015). https://doi.org/10.1063/pt.3.2845
19. J. Qi, T. Li, R. Xu et al., α decay in intense laser fields: calculations using realistic nuclear potentials. Phys. Rev. C **99**, 044610 (2019). https://doi.org/10.1103/PhysRevC.99.044610
20. A. Pálffy, S.V. Popruzhenko, Can extreme electromagnetic fields accelerate the α decay of nuclei? Phys. Rev. Lett. **124**, 212505 (2020). https://doi.org/10.1103/PhysRevLett.124.212505
21. D. Bai, Z. Ren, Decays in superstrong static electric fields. Commun. Theor. Phys. **70**, 559 (2018). https://doi.org/10.1088/0253-6102/70/5/559
22. J. Cheng, W. Zhang, Q. Xiao et al., Determinants in laser-assisted deformed α decay. Phys. Lett. B **848**, 138322 (2024). https://doi.org/10.1016/j.physletb.2023.138322

23. J. Qi, L. Fu, X. Wang, Nuclear fission in intense laser fields. Phys. Rev. C **102**, 064629 (2020). https://doi.org/10.1103/PhysRevC.102.064629
24. R. Röhlsberger, K. Schlage, B. Sahoo et al., Collective Lamb shift in single-photon superradiance. Science **328**, 1248 (2010). https://doi.org/10.1126/science.1187770
25. R. Röhlsberger, H. Wille, K. Schlage et al., Electromagnetically induced transparency with resonant nuclei in a cavity. Nature **482**, 199 (2012). https://doi.org/10.1038/nature10741
26. F. Vagizov, V. Antonov, Y.V. Radeonychev et al., Coherent control of the waveforms of recoilless γ-ray photons. Nature **508**, 80 (2014). https://doi.org/10.1038/nature13018
27. K.P. Heeg, A. Kaldun, C. Strohm et al., Coherent X-ray-optical control of nuclear excitons. Nature **590**, 401 (2021). https://doi.org/10.1038/s41586-021-03276-x
28. T. Li, X. Wang, Nonlinear optical effects in a nucleus. J. Phys. G **48**, 095105 (2021). https://doi.org/10.1088/1361-6471/ac1712
29. H. Zhang, T. Li, X. Wang, Highly nonlinear light-nucleus interaction. Phys. Rev. Lett. **133**, 152503 (2024). https://doi.org/10.1103/PhysRevLett.133.152503
30. X. Liu, Triggering highly nonlinear responses in ^{229}Th nuclei with an intense laser. Nucl. Sci. Tech. **36**, 20 (2025). https://doi.org/10.1007/s41365-024-01632-w
31. I. Pomerantz, E. McCary, A.R. Meadows et al., An ultra-short pulsed neutron source. Phys. Rev. Lett. **113**, 184801 (2014). https://doi.org/10.1103/PhysRevLett.113.184801
32. Y. Shou, X. Wu, K.H. Pae et al., Laser-driven proton acceleration beyond 100 MeV by radiation pressure and Coulomb repulsion in a conduction-restricted plasma. Nat. Commun. **16**, 1487 (2025). https://doi.org/10.1038/s41467-025-56667-3
33. F. Zhang, L. Deng, Y. Ge et al., First proof of principle experiment for muon production with ultrashort high intensity laser. Nat. Phys. **21**, 1050 (2025). https://doi.org/10.1038/s41567-025-02872-2
34. J. Feng, J. Qi, H. Zhang et al., Laser-based approach to measure small nuclear cross sections in plasma. P. Natl. Acad. Sci. USA **121**, e2413221121 (2024). https://doi.org/10.1073/pnas.2413221121
35. W. Wang, C. Lv, X. Zhang et al., First measurement of the ^{7}Li(D, n) astrophysical S-factor in laser-induced full plasma. Phys. Lett. B **843**, 10 (2023). https://doi.org/10.1016/j.physletb.2023.138034
36. W. Liu, B. Guo, Z. An et al., Recent progress in nuclear astrophysics research and its astrophysical implications at the China Institute of Atomic Energy. Nucl. Sci. Tech. **35**, 217 (2024). https://doi.org/10.1007/s41365-024-01590-3
37. T. Masuda, A. Yoshimi, A. Fujieda et al., X-ray pumping of the ^{229}Th nuclear clock isomer. Nature **573**, 238 (2019). https://doi.org/10.1038/s41586-019-1542-3
38. W. Wang, J. Zhou, B. Liu et al., Exciting the isomeric ^{229}Th nuclear state via laser-driven electron recollision. Phys. Rev. Lett. **127**, 052501 (2021). https://doi.org/10.1103/PhysRevLett.127.052501
39. Y. Wu, J. Gunst, C.H. Keitel et al., Tailoring laser-generated plasmas for efficient nuclear excitation by electron capture. Phys. Rev. Lett. **120**, 052504 (2018). https://doi.org/10.1103/PhysRevLett.120.052504
40. J. Feng, W. Wang, C. Fu et al., Femtosecond pumping of nuclear isomeric states by the Coulomb collision of ions with quivering electrons. Phys. Rev. Lett. **128**, 052501 (2022). https://doi.org/10.1103/PhysRevLett.128.052501
41. J. Qi, H. Zhang, X. Wang, Isomeric excitation of ^{229}Th in laser-heated clusters. Phys. Rev. Lett. **130**, 112501 (2023). https://doi.org/10.1103/PhysRevLett.130.112501
42. J. Tiedau, M.V. Okhapkin, K. Zhang et al., Laser excitation of the Th-229 nucleus. Phys. Rev. Lett. **132**, 182501 (2024). https://doi.org/10.1103/PhysRevLett.132.182501
43. R. Elwell, C. Schneider, J. Jeet et al., Laser excitation of the ^{229}Th nuclear isomeric transition in a solid-state host. Phys. Rev. Lett. **133**, 013201 (2024). https://doi.org/10.1103/PhysRevLett.133.013201
44. C. Zhang, T. Ooi, J.S. Higgins et al., Frequency ratio of the ^{229m}Th nuclear isomeric transition and the ^{87}Sr atomic clock. Nature (London) **633**, 63 (2024). https://doi.org/10.1038/s41586-024-07839-6
45. C. Kohlfürst, F. Queisser, R. Schützhold, Dynamically assisted tunneling in the impulse regime. Phys. Rev. Res. **3**, 033153 (2021). https://doi.org/10.1103/PhysRevResearch.3.033153
46. J.J. Bekx, M.L. Lindsey, S.H. Glenzer et al., Applicability of semiclassical methods for modeling laser-enhanced fusion rates in a realistic setting. Phys. Rev. C **105**, 054001 (2022). https://doi.org/10.1103/PhysRevC.105.054001
47. J.J. Bekx, M.L. Lindsey, K.G. Schlesinger, Effect of nuclear charge on laser-induced fusion enhancement in advanced fusion fuels. Phys. Rev. C **106**, 034003 (2022). https://doi.org/10.1103/PhysRevC.106.034003
48. M.L. Lindsey, J.J. Bekx, K.G. Schlesinger et al., Dynamically assisted nuclear fusion in the strong-field regime. Phys. Rev. C **109**, 044605 (2024). https://doi.org/10.1103/PhysRevC.109.044605
49. J.J. Bekx, S.H. Glenzer, K.G. Schlesinger, Laser-enhanced fusion burn fractions for advanced fuels. Phys. Rev. C **110**, 024612 (2024). https://doi.org/10.1103/PhysRevC.110.024612
50. E.M. Burbidge, G.R. Burbidge, W.A. Fowler et al., Synthesis of the elements in stars. Rev. Mod. Phys. **29**, 547 (1957). https://doi.org/10.1103/RevModPhys.29.547
51. G. Gamow, Zur quantentheorie des atomkernes. Z. Phys. **51**, 204 (1928). https://doi.org/10.1007/bf01343196
52. H.S. Bosch, G.M. Hale, Improved formulas for fusion cross-sections and thermal reactivities. Nucl. Fusion **32**, 611 (1992). https://doi.org/10.1088/0029-5515/32/4/i07
53. D.M. Volkov, The solution for wave equations for a spin-charged particle moving in a classical field. Z. Phys. **94**, 250 (1935)
54. V.S. Belyaev, A.P. Matafonov, V.I. Vinogradov et al., Observation of neutronless fusion reactions in picosecond laser plasmas. Phys. Rev. E **72**, 026406 (2005). https://doi.org/10.1103/PhysRevE.72.026406
55. C. Labaune, C. Baccou, S. Deprierraux et al., Fusion reactions initiated by laser-accelerated particle beams in a laser-produced plasma. Nat. Commun. **4**, 2506 (2013). https://doi.org/10.1038/ncomms3506
56. A. Picciotto, D. Margarone, A. Velyhan et al., Boron-proton nuclear-fusion enhancement induced in boron-doped silicon targets by low-contrast pulsed laser. Phys. Rev. X **4**, 031030 (2014). https://doi.org/10.1103/PhysRevX.4.031030
57. S. Eliezer, H. Hora, G. Korn et al., Response to "Comment on 'Avalanche proton-boron fusion based on elastic nuclear collisions' " [Phys. Plasmas 23, 094703 (2016)]. Phys. Plasmas **23**, 094704 (2016). https://doi.org/10.1063/1.4963007
58. F. Belloni, D. Margarone, A. Picciotto et al., On the enhancement of p-^{11}B fusion reaction rate in laser-driven plasma by $\alpha \rightarrow$p collisional energy transfer. Phys. Plasmas **25**, 020701 (2018). https://doi.org/10.1063/1.5007923
59. A. Tentori, F. Belloni, Revisiting p-^{11}B fusion cross section and reactivity, and their analytic approximations. Nucl. Fusion **63**, 086001 (2023). https://doi.org/10.1088/1741-4326/acda4b
60. L.V. Keldysh, Ionization in the field of a strong electromagnetic wave. Sov. Phys. JETP **20**, 1307 (1965). https://doi.org/10.1142/9789811279461_0008
61. M.V. Ammosov, N.B. Delone, V.P. Krainov, Tunnel ionization of complex atoms and atomic ions in electromagnetic field. Sov. Phys. JETP **64**, 1191 (1986). https://doi.org/10.1117/12.938695

62. M. Jain, N. Tzoar, Compton scattering in the presence of coherent electromagnetic radiation. Phys. Rev. A **18**, 538 (1978). https://doi.org/10.1103/PhysRevA.18.538
63. F.H.M. Faisal, Strong-field S-matrix theory with final-state Coulomb interaction in all orders. Phys. Rev. A **94**, 031401(R) (2016). https://doi.org/10.1103/PhysRevA.94.031401